

Dynamic Average Modeling of Front-End Diode Rectifier Loads Considering Discontinuous Conduction Mode and Unbalanced Operation

IEEE Task Force on Dynamic Average Modeling

S. Chiniforoosh, H. Atighechi, A. Davoudi, J. Jatskevich (Task Force Chair), A. Yazdani, S. Filizadeh, M. Saeedifard, J. A. Martinez, V. Sood, K. Strunz, J. Mahseredjian, and V. Dinavahi

Abstract—Electric power distribution systems of many commercial and industrial sites often employ variable frequency drives and other loads that internally utilize dc. Such loads are often based on front-end line-commutated rectifiers. The detailed switch-level models of such rectifier systems can be readily implemented using a number of widely available digital programs and transient simulation tools, including the Electromagnetic Transient (EMT)-based programs and Matlab/Simulink. To improve the simulation efficiency for the system-level transient studies with a large number of such subsystems, the so-called dynamic average models have been utilized. This paper presents the average-value modeling methodologies for the conventional three-phase (six-pulse) front-end rectifier loads. We demonstrate the system operation and the dynamic performance of the developed average models in discontinuous and continuous modes, as well as under balanced and unbalanced operation.

Index Terms—Average-value modeling, digital simulation, line-commutated converters, operational modes, rectifiers.

I. INTRODUCTION

THE conventional three-phase (six-pulse) line-commutated rectifiers are commonly found as the input stage in low-to medium-power variable frequency drives and motor loads that are widely used in industrial and commercial applications [1]–[7]. These loads are often referred to as the front-end rectifier loads [8], [9], and may appear in large numbers in distribution systems, industrial facilities [10], distributed generation [11], transportation [12], as well as arc furnaces [13], [14]. A typical configuration considered in this paper is shown in Fig. 1. Depending on the application, the source may be a distribution feeder (or transformer) as in Case I, or a rotating machine (generator) as in Case II. The ac filter network may take various configurations depending on application and cost constraints, wherein phase-shifting transformers, passive or active filters may be considered to reduce the harmonics. Commonly used passive filters include series choke inductors and the shunt filters that are tuned to lower harmonics (typically 5th and 7th) [15], [16].

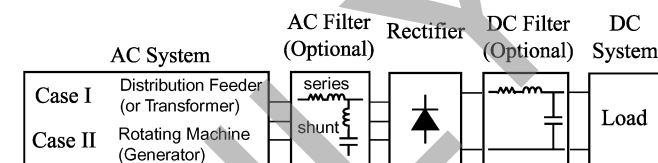


Fig. 1. Typical configuration of a front-end rectifier load system.

The ac filter network may take various configurations depending on application and cost constraints, wherein phase-shifting transformers, passive or active filters may be considered to reduce the harmonics. Commonly used passive filters include series choke inductors and the shunt filters that are tuned to lower harmonics (typically 5th and 7th) [15], [16].

The modeling of rectifier systems has been of particular interest to the power engineering community for a long time [17], [18]. The detailed modeling of power systems that contain rectifier loads may be readily carried out using digital programs such as the Alternate Transients Program (ATP) [19], EMTP-RV [20], PSCAD/EMTDC [21], Matlab/Simulink [22], etc. The main challenge of using the detailed models is the increased computational complexity which leads to longer simulation times especially when the overall system contains many rectifiers and switching modules.

Dynamic average modeling has been utilized as a mean of removing the high-frequency switching from the model while preserving the lower frequency dynamics [23]. This Task Force paper describes the variations of the six-pulse rectifier system depicted in Fig. 1 that are commonly encountered in practical applications leading to discontinuous and continuous conduction modes (DCM and CCM), respectively. The basic approaches to develop appropriate dynamic average models are also presented. The transient performance of several example models is demonstrated for various operating conditions, including light and heavy loading conditions, discontinuous and continuous modes, as well as balanced and unbalanced ac side. The dynamic model of front-end rectifiers with unbalanced input voltages is particularly desirable when studying single-phase faults and voltage sags [24].

II. MODES OF OPERATION

To set the stage for discussing the system operation and modeling, a simplified circuit diagram for the front-end rectifier load

Manuscript received August 31, 2011; accepted September 09, 2011. Date of publication October 25, 2011; date of current version December 23, 2011. Paper no. TPWRD-00741-2011.

The Task Force on Dynamic Average Modeling is with the Working Group on Modeling and Analysis of System Transients Using Digital Programs.

Task force members: S. A. Abdulsalam, U. Annakkage, H. Atighechi, J. Belanger, S. Chiniforoosh, A. Davoudi, V. Dinavahi, O. Faruque, S. Filizadeh, D. Goldsworthy, A. Gole, R. Iravani, J. Jatskevich (Task Force Chair), R. Jayasinghe, H. Karimi, M. Kuschke, A. St. Leger, J. Mahseredjian, J. Martinez, N. Nair, L. Naredo, T. Noda, J. N. Paquih, J. Peralta, A. Ramirez, A. Rezaei-Zare, M. Rioual, M. Saeedifard, K. Schoder, V. Sood, K. Strunz, A. VanDerMeer, A. Yazdani.

Color versions of one or more of the figures in this paper are available online at <http://ieeexplore.ieee.org>.

Digital Object Identifier 10.1109/TPWRD.2011.2168983

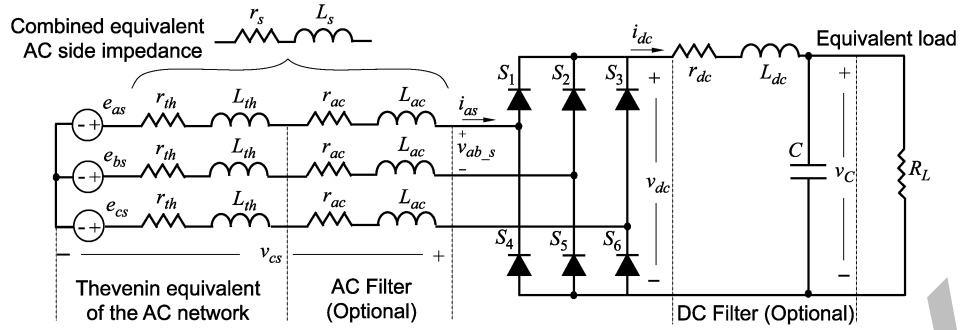


Fig. 2. Simplified circuit diagram of a typical three-phase front-end rectifier load system.

system considered in this paper is depicted in Fig. 2. Since the presence of shunt filters does not change the development of dynamic average models in general, only series filters are considered here. The ac network is represented by its Thevenin equivalent voltages e_{abc} , series resistance r_{th} and inductance L_{th} . The impedance of an optional series ac filter is represented by r_{ac} , L_{ac} . The combined equivalent impedance of the ac subsystem is denoted by r_s and L_s , respectively. The dc filter represented in Fig. 2 by r_{dc} , L_{dc} , and C is also optional and may be partially present in the system.

If the system is fed from a synchronous generator (Fig. 1 Case II), the machine can be represented using the voltage-behind-reactance formulation, which results in a circuit similar to Fig. 2 (but possibly with coupled and/or variable equivalent inductances) [25]–[27]. In many cases, such as battery charging [28], [29] and variable-speed-drive applications [8], [9], the dc filter inductor may be omitted, whereas the capacitor is included to smooth the dc bus voltage. The ac filter inductor must often be included in order to reduce the ac-side current harmonics.

To represent an equivalent energy dissipating load on the dc side in Fig. 2, a simple resistor R_L is connected to the dc bus [28], [30], [31]. Although such an assumption ignores the interharmonics [32], it is deemed acceptable in lower power applications [33], [34], and is considered sufficient for the purpose of this paper.

In this system, a discontinuous conduction mode (DCM) operation is typically observed at light load. This mode is frequently encountered in the front-end rectifiers of low- to medium power variable frequency drives [30], [32], where the ac filter is often not used (or is very small) but there is a significant capacitor on the dc bus. The corresponding waveforms are illustrated in Fig. 3(a). There, six equal switching intervals exist within a single electrical cycle. In DCM, each switching interval is divided into two subintervals. During the conduction subinterval, t_{cond} , two diodes are conducting and two of the phases carry the dc bus current in opposite directions. At some point, the line-to-line voltage in these two phases becomes smaller than the dc bus voltage and the current reaches zero and remains zero for the rest of the interval—hence discontinuous mode. This subinterval is denoted by t_{dcm} in Fig. 3(a). During t_{dcm} , all diodes are off. The dc load is, meanwhile, being fed from the dc capacitor as observed in the dc bus voltage waveform v_{dc} . The switching pattern in the DCM is therefore 2-0.

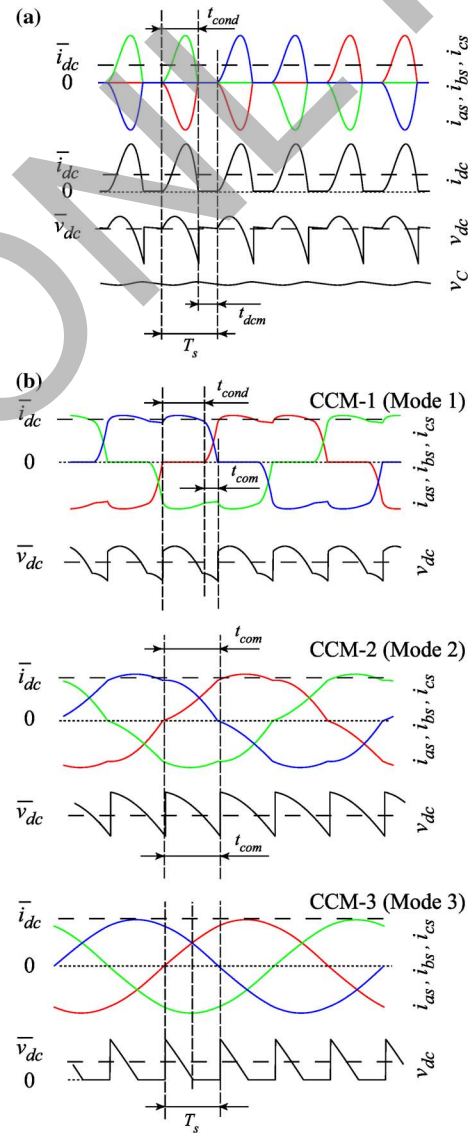


Fig. 3. Typical current and voltage waveforms of the six-pulse rectifier. (a) Operation in DCM. (b) Operation in CCM.

If the combined value of the source and ac filter inductances becomes sufficiently large [30], [35], or the load on the dc bus is sufficiently increased, the dc bus current becomes continuous—hence continuous mode. In this case, as the load varies

TABLE I
OPERATIONAL MODES OF THE CONVENTIONAL
THREE-PHASE (6-PULSE) RECTIFIER

Operational Modes	Conduction Pattern	Commutation Angle
DCM	2-0	$\mu = 0^\circ$
CCM-1	2-3	$0^\circ < \mu < 60^\circ$
CCM-2	3	$\mu = 60^\circ$
CCM-3	3-4	$60^\circ < \mu < 120^\circ$

from a light load to a short circuit, three different switching patterns can be observed, resulting in three distinct continuous conduction modes (CCM) of operation [36]. The typical waveforms of the phase currents and the corresponding dc bus voltages are shown in Fig. 3(b). The operational modes are summarized in Table I, together with the conduction pattern and the commutation angle.

Within CCM-1 [see Fig. 3(b), top plot], each switching interval is divided into two subintervals referred to as commutation and conduction [37]. During the conduction subinterval t_{cond} , only two diodes conduct; whereas during the commutation subinterval t_{com} , corresponding to the commutation angle $\mu = \omega_e \cdot t_{\text{com}}$, the current is being switched from one phase to another and three diodes conduct. Therefore, a conduction pattern of 2–3 diodes is observed within each 60 electrical degrees, and $0^\circ < \mu < 60^\circ$.

The mode CCM-2 [see Fig. 3(b), middle plot], may be achieved by further increasing the load current. In this mode, the commutation angle μ increases and reaches 60° , resulting in the disappearance of the conduction subinterval. Consequently, there will be three diodes carrying current throughout the switching intervals. Hence, the conduction pattern becomes just 3 (or 3-3).

If the load current is further increased, the commutation angle μ starts to increase, resulting in the third mode, CCM-3 [see Fig. 3(b), bottom plot]. This changes the switching pattern to 3–4 conducting diodes. Note that this mode contains a topology with four simultaneously conducting diodes, which short-circuits the output as observed in Fig. 3(b), (bottom plot). This last mode rarely occurs in practical systems, but it is possible in rotating machines and brushless exciters with very large inductances [38].

Certain variations in topology of the system of Fig. 2 may prevent the occurrence of some of the operational modes. For instance, without the dc filter inductor, the CCM-3 mode cannot occur and the system could only operate in DCM, CCM-1, or CCM-2. Comparing the phase currents in DCM depicted in Fig. 3(a), it can also be concluded that such currents will inject significant harmonics into the network. To avoid operation in DCM, medium and large drives with front-end rectifiers often install additional ac filters (series inductors and shunt filters) to shift the operation to CCM-1 or CCM-2.

III. DYNAMIC AVERAGE MODELING

The dynamic average models for the six-pulse converters can be generally developed using two main approaches (i.e., analytical [37], [39]–[43] and parametric [44], [45]). Using the first

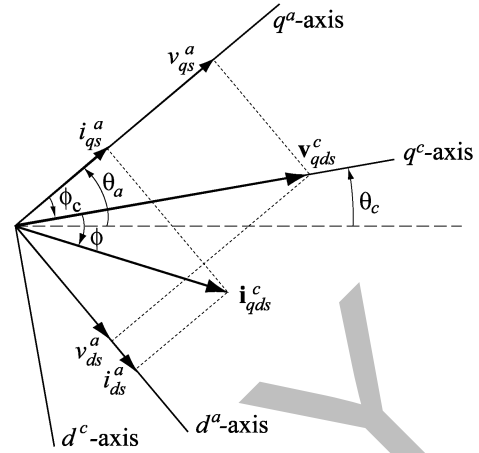


Fig. 4. Relationship among the variables in the converter and the arbitrary reference frames.

approach, the system variables are analytically averaged over a prototypical switching interval [37], and the system state and algebraic equations are derived. The fast averaging over a prototypical switching interval T_s is defined as

$$\bar{f}(t) = \frac{1}{T_s} \int_{t-T_s}^t f(\tau) d\tau \quad (1)$$

where f is a network variable (e.g., voltage or current) and \bar{f} is the so-called fast average of f . While the definition (1) may be directly applied to the dc variables, the ac variables first have to be transformed into an appropriate synchronously rotating reference frame [37]. Here, we adopt the qd -reference frame convention where the q axis is leading the d axis by 90° [37]. In this reference frame, the resulting qd variables in steady state are composed of a constant (dc) component and a ripple. The averaging of these variables using (1) removes the switching ripple but preserves the slower (dc) variations of the transformed variables. The converter reference frame is typically chosen wherein the d axis component of voltage is zero as depicted in Fig. 4.

The relationship between the voltages in the converter and arbitrary reference frames may be written as

$$\begin{bmatrix} v_{qs}^c \\ 0 \end{bmatrix} = \begin{bmatrix} \cos(\phi_c) & \sin(\phi_c) \\ -\sin(\phi_c) & \cos(\phi_c) \end{bmatrix} \begin{bmatrix} v_{qs}^a \\ v_{ds}^a \end{bmatrix}. \quad (2)$$

The angle between the converter and arbitrary reference frames may also be deduced from Fig. 4 as

$$\phi_c = \tan^{-1} \left(\frac{v_{ds}^a}{v_{qs}^a} \right). \quad (3)$$

Table II lists various dynamic average models present in the literature for the six-pulse system together with the list of features included in each model. The first challenge in deriving the AVMs analytically is the existence of various operational modes discussed previously. The AVM is typically considered for the most common mode of operation (i.e., CCM-1). In order to extend such models to all modes, the corresponding equations for each mode must be derived and averaged using a similar procedure. Moreover, the boundary conditions for each of the modes should be established. Therefore, there will be an AVM valid

TABLE II
AVERAGE MODELS OF THE THREE-PHASE RECTIFIER SYSTEMS

Models	steady-state/ dynamic	dynamic order (full/reduced)	DCM, CCMs (1, 2, 3)	ac filter (r_{ac} , L_{ac})	dc filter (r_{dc} , L_{dc} , C)	variable ac inductance (yes/no)
[37]	dynamic	reduced	CCM 1	L_{ac}	r_{dc} , L_{dc} , C	no
[46]	dynamic	reduced	CCM 2	r_{ac} , L_{ac}	C	no
[47]	dynamic	reduced	CCM 2	L_{ac}	C	no
[39], [40]	dynamic	reduced	CCM 1	r_{ac} , L_{ac}	r_{dc} , L_{dc} , C	no
[41]	steady-state	N/A	CCM 1	-	r_{dc} , L_{dc} , C	yes
[42]	dynamic	reduced	CCM 1	-	r_{dc} , L_{dc} , C	yes
[43]	dynamic	reduced	CCM 1	-	C	yes
[44]	dynamic	full	CCM 1	-	C	yes
[38]	dynamic	reduced	CCMs 1, 2, 3	-	r_{dc} , L_{dc} , C	yes
[45]	dynamic	full	CCMs 1, 2, 3	-	r_{dc} , L_{dc} , C	yes

for each operational mode that is in the range of interest. These models can then be “switched” as the system changes modes, which makes this approach additionally challenging.

Other challenges of the analytical approach include the difficulty of establishing closed-form explicit equations describing the system in more complicated configurations (e.g., machine-fed converter systems) (Case II in Fig. 1) [41]–[43]. In many cases, the final model will be implicit and would require an iterative solution. Analytically derived AVMs have been formulated in [37], [39], [40], and [41]–[43] for voltage-source- and machine-fed converters, respectively. The model [37], for example, in addition to only being valid in CCM-1 mode, also neglects the resistance on the ac side r_s in Fig. 2. Subsequent improvements have been done in [39] to include the ac-side resistance and improve the model dynamics. The particular case of three-phase rectifier feeding constant-voltage loads has been addressed in [46] and [47]. A parametric approach has been considered in [44] and [45]. An extension of this method to more general cases and topologies is rather straightforward. Recent work also includes the average modeling of power-electronic systems using polynomial chaos basis [48].

IV. EXAMPLES OF BASIC AVERAGE-VALUE MODELS

Among various models provided in Table II, three basic models are considered in this paper.

A. Classical Reduced-Order Model (AVM-1)

The classical model [37] requires the state equation that describes the dc bus current dynamics as

$$\frac{d\bar{i}_{dc}}{dt} = \frac{\frac{3\sqrt{3}}{\pi}\sqrt{2}E - \left(\frac{3}{\pi}\omega_e L_s + r_{dc}\right)\bar{i}_{dc} - v_C}{2L_s + L_{dc}} \quad (4)$$

where E is the rms value of the phase voltage, and v_C is the dc bus voltage on the filter capacitor.

To establish the average q and d axes components of the phase currents, the dc current is assumed constant and equal to its average value during the switching interval. The current dynamics

disappear, resulting in a reduced-order model. The phase currents are then expressed during conduction and commutation subintervals and are averaged, respectively. The result of this procedure yields the following equations:

$$\begin{aligned} \bar{i}_{qs,com}^c &= \frac{-2\sqrt{3}\tau}{\pi} i_{dc} \left[\sin\left(\mu - \frac{5\pi}{6}\right) + \sin\left(\frac{5\pi}{6}\right) \right] \\ &\quad - \frac{3\sqrt{2}E}{\pi\omega_e L_s} (\cos\mu - 1) \\ &\quad + \frac{3\sqrt{2}E}{4\pi\omega_e L_s} (\cos(2\mu) - 1), \end{aligned} \quad (5)$$

$$\begin{aligned} \bar{i}_{ds,com}^c &= \frac{-2\sqrt{3}\tau}{\pi} i_{dc} \left[\cos\left(\frac{5\pi}{6}\right) - \cos\left(\mu - \frac{5\pi}{6}\right) \right] \\ &\quad - \frac{3\sqrt{2}E}{\pi\omega_e L_s} \sin\mu + \frac{3\sqrt{2}E}{4\pi\omega_e L_s} (\sin(2\mu) + 2\mu), \end{aligned} \quad (6)$$

$$\bar{i}_{qs,cond}^c = \frac{-2\sqrt{3}\tau}{\pi} i_{dc} \left[\sin\left(\frac{7\pi}{6}\right) - \sin\left(\mu + \frac{5\pi}{6}\right) \right], \quad (7)$$

$$\bar{i}_{ds,cond}^c = \frac{-2\sqrt{3}\tau}{\pi} i_{dc} \left[\cos\left(\mu + \frac{5\pi}{6}\right) - \cos\left(\frac{7\pi}{6}\right) \right]. \quad (8)$$

The final averaged ac-side currents are obtained as

$$\bar{i}_{qs}^c = \bar{i}_{qs,com}^c + \bar{i}_{qs,cond}^c, \quad (9)$$

$$\bar{i}_{ds}^c = \bar{i}_{ds,com}^c + \bar{i}_{ds,cond}^c. \quad (10)$$

The model defined by (4)–(10) is referred to as AVM-1.

B. Improved Reduced-Order Model (AVM-2)

A similar model has been derived in [39]; where instead of assuming a constant value for the dc current during the switching interval, this current is assumed to change as

$$i_{dc}(\theta) = i_{dc0} + k \cdot \left(\theta - \frac{\mu}{2}\right) \quad (11)$$

where i_{dc0} is the average value of i_{dc} during the commutation period, and k is the derivative $di_{dc}/d\theta_e$ during this period of

time. The effect of ac-side resistance has been also partly taken into account. The resulting model has the following form:

$$\left[\frac{\pi}{3} - \mu + \frac{3\mu^2}{4\pi} r_s + \frac{4\pi - 3\mu}{2\pi} L_s + \frac{\pi}{3} - \mu \right] \frac{di_{dc}}{dt} = \frac{3\sqrt{3}}{\pi} \sqrt{2} E \left(1 - \frac{r_s}{\omega_e L_s} \frac{\mu - \sin \mu}{2} \right) - \left(\frac{2\pi - 3\mu}{\pi} r_s + \frac{3}{\pi} \omega_e L_s + r_{dc} \right) i_{dc0} - v_C \quad (12)$$

$$\bar{i}_{qs}^c = -\frac{2\sqrt{3}}{\pi} i_{dc0} \cos \mu + \frac{\sqrt{3}}{\pi} k \left(-\sin \mu + \frac{\pi}{3} \right) + \frac{3}{\pi} \frac{\sqrt{2} E}{\omega_e L_s} \left(\cos \mu - \frac{\cos(2\mu)}{4} - \frac{3}{4} \right) \quad (13)$$

$$\bar{i}_{ds}^c = -\frac{2\sqrt{3}}{\pi} i_{dc0} \sin \mu + \frac{\sqrt{3}}{\pi} k \left(\cos \mu + 1 - \frac{\sqrt{3}\pi}{3} \right) + \frac{3}{\pi} \frac{\sqrt{2} E}{\omega_e L_s} \left(\sin \mu - \frac{\sin(2\mu)}{4} - \frac{\mu}{2} \right). \quad (14)$$

The model defined by (12)–(14) is referred to as AVM-2. Both AVM-1 and AVM-2 utilize the same commutation angle

$$\mu = \cos^{-1} \left(1 - \frac{\sqrt{2} \omega_e L_s \bar{i}_{dc}}{\sqrt{3} E} \right). \quad (15)$$

C. Parametric Average-Value Model (PAVM)

In parametric approach [45], the rectifier switching cell is considered as an algebraic block that relates the dc voltage and current \bar{v}_{dc} , \bar{i}_{dc} to the ac voltages and currents $\bar{\mathbf{v}}_{qds}^c$ and $\bar{\mathbf{i}}_{qds}^c$ through the respective parametric functions as

$$\|\bar{\mathbf{v}}_{qds}^c\| = \alpha(\cdot) \bar{v}_{dc}, \quad (16)$$

$$\bar{i}_{dc} = \beta(\cdot) \|\bar{\mathbf{i}}_{qds}^c\| \quad (17)$$

where $\alpha(\cdot)$ and $\beta(\cdot)$ are algebraic functions of the loading conditions. To complete this model, the angle between the vectors $\bar{\mathbf{v}}_{qds}^c$ and $\bar{\mathbf{i}}_{qds}^c$ is calculated based on Fig. 4 as

$$\phi(\cdot) = \tan^{-1} \left(\frac{\bar{v}_{ds}^a}{\bar{v}_{qs}^a} \right) - \tan^{-1} \left(\frac{\bar{i}_{ds}^a}{\bar{i}_{qs}^a} \right). \quad (18)$$

Deriving closed-form analytical expressions for $\alpha(\cdot)$, $\beta(\cdot)$, and $\phi(\cdot)$ is impractical. Instead, these functions may be extracted by using the simulation and expressed in terms of dynamic impedance of the switching cell defined as [45]

$$z = \frac{\bar{v}_{dc}}{\|\bar{\mathbf{i}}_{qds}^c\|}. \quad (19)$$

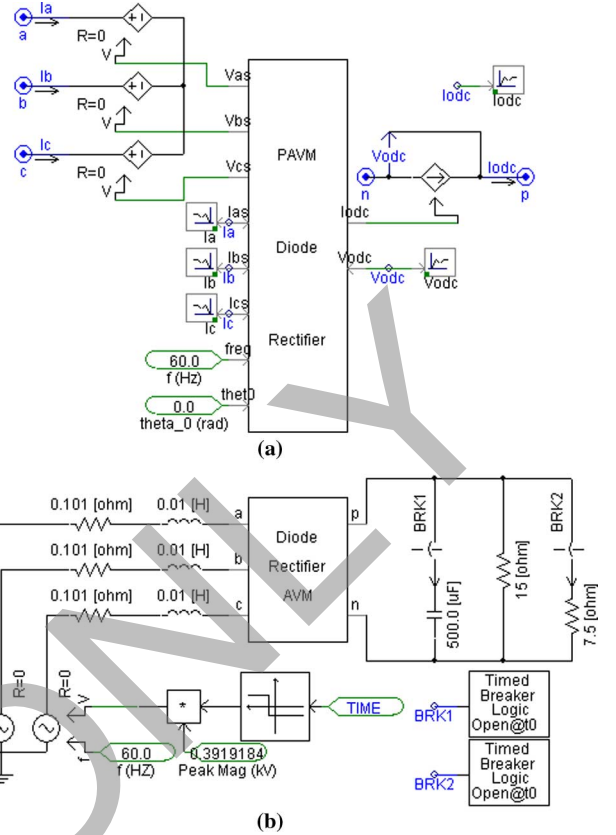


Fig. 5. Example of parametric average-value model implemented in PSCAD. (a) PAVM block together with controllable sources and interfacing ports. (b) AVM module interfaced with external ac and dc subsystems.

V. EXAMPLE OF AVM IMPLEMENTATION IN PSCAD

In this paper, PSCAD/EMTDC, EMTP-RV, and Matlab/Simulink have been used to implement the considered models. The results predicted by all packages are essentially identical, provided the time step and solver properties are chosen appropriately. The system parameters are summarized in the Appendix.

To illustrate the use of AVM in EMTP-type packages, an example implementation of the PAVM in PSCAD is shown in Fig. 5. The block shown in Fig. 5(a) contains (16)–(19) and the transformations between qd and abc coordinates. To interface the AVM with the external ac network, three controllable voltage sources are used whose values are determined by (16) transformed into abc coordinates. The dc side is interfaced using a controllable current source whose value is determined by (17). The values of the ac currents and the dc voltage are read from the network solution and taken as the inputs into the algebraic block, wherein the ac currents are transformed into qd coordinates for use in (17). The subsystem of Fig. 5(a) is encapsulated into a single module block that is then interconnected using its nodes with the external network as shown in Fig. 5(b). This AVM block can then replace the detailed switching rectifier module within a larger ac and dc network (which may include ac filters, for example, shunt harmonic filters, etc.). Fig. 5(b) also depicts the timed breaker blocks that are used to implement the system changes.

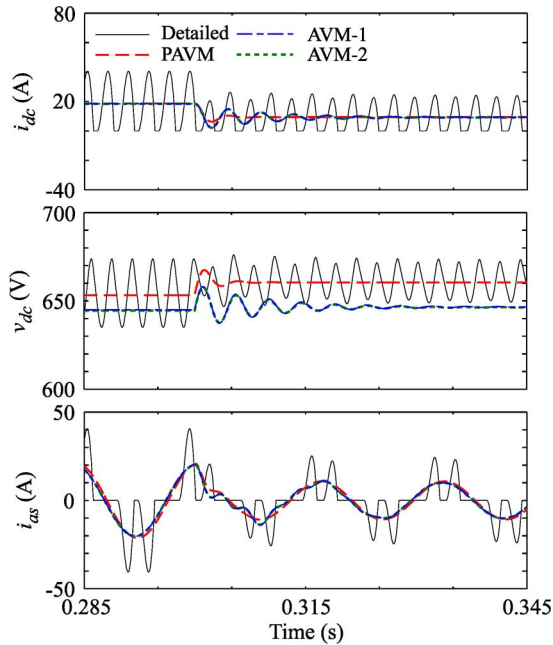


Fig. 6. Transient response of the six-pulse rectifier system in DCM.

VI. DYNAMIC PERFORMANCE UNDER BALANCED CONDITIONS

A. Operation in DCM

The rectifier system is assumed to operate without the ac filter but with the dc capacitor in order to enable the DCM. In the following study, the system initially operates in steady state in DCM with load $R_L = 35 \Omega$. At $t = 0.3$ s, the load resistance is stepped to $R_L = 70 \Omega$, which forces the system deeper into the DCM operation at a lighter load. The transient responses obtained by the considered detailed and average models are shown in Fig. 6. The analytical models AVM-1 and AVM-2 predict the dc and ac currents with reasonable accuracy, including the change in operating conditions. The PAVM shows somewhat higher damping than the other models but with a superior prediction of the dc voltage.

B. Operation in CCM

To investigate the performance in CCM, the ac series filter is added. In the following study, the system is assumed to start from zero initial conditions in CCM-1 with the load $R_L = 11.9 \Omega$. At $t = 0.05$ s, the load is stepped to $R_L = 2 \Omega$ forcing the system into the CCM-2 [see Fig. 3(b)]. The resulting transient response predicted by various models is shown in Fig. 7. This figure clearly shows that although AVM-1 and AVM-2 have been derived for CCM-1, their transient response does not exactly follow the dynamic response of the detailed model. The improved model AVM-2 predicts the transient slightly better than the classical model AVM-1. The PAVM perfectly follows the initialization transient including the overshoot oscillations. At $t = 0.05$ s, the rectifier system undergoes another transient and transitions into CCM-2. Both AVM-1 and AVM-2 clearly do not follow this transition very well and predict higher dc voltage and current. However, the response of the full-order

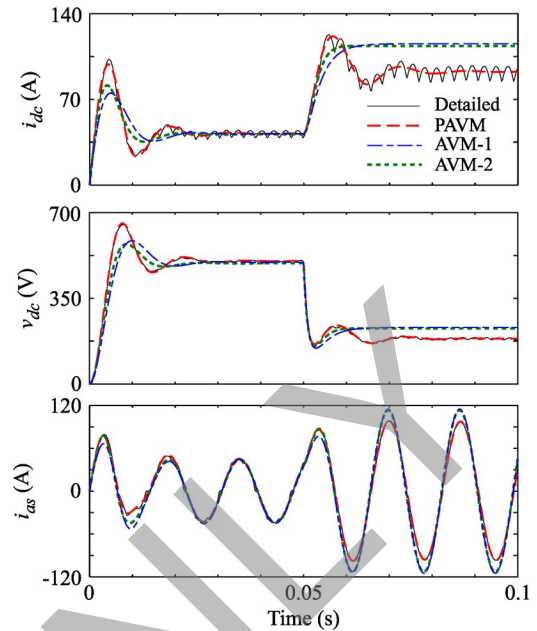


Fig. 7. Transient response of the six-pulse rectifier system with the dc capacitor.

PAVM model is very much consistent with the transient and new steady state predicted by the detailed model.

VII. PERFORMANCE UNDER UNBALANCED CONDITIONS

In this section, the performance of the detailed and average models under an unbalanced condition is demonstrated. It is very desirable to have the average models that are capable of accurately predicting the result of the ac network unbalance and its impact on the ac and dc sides of the system in DCM and CCM.

A. Unbalanced Operation in DCM

For implementing the DCM operation, the ac input filter is removed and the dc capacitor is added to the rectifier system. In the following study, the rectifier system initially operates under a balanced condition with a resistive load of $R_L = 20 \Omega$. This operating point is close to the boundary between DCM and CCM-1. At $t = 0.08$ s, a phase shift of 45° in the c -phase voltage e_{cs} is introduced, making the three phases asymmetric. This change in input voltage throws the rectifier system into unbalanced operation in DCM. Next, at $t = 0.11$ s, the load is stepped to $R_L = 50 \Omega$ making the DCM operation even lighter. The corresponding transient responses are shown in Figs. 8 and 9. As can be seen in Fig. 8, the heavy asymmetry of the input ac voltages leads to a pronounced change in the conduction pattern of the rectifier diodes, making the ac currents particularly spiky and uneven among the phases. The resulting dc current and voltage are shown in Fig. 9. It can be observed in Figs. 8 and 9 that the models AVM-1 and AVM-2 do not predict this condition well by producing larger ripple in dc voltage and current. At the same time, PAVM appears to predict the dc variables with much greater accuracy, closely resembling the peaks and

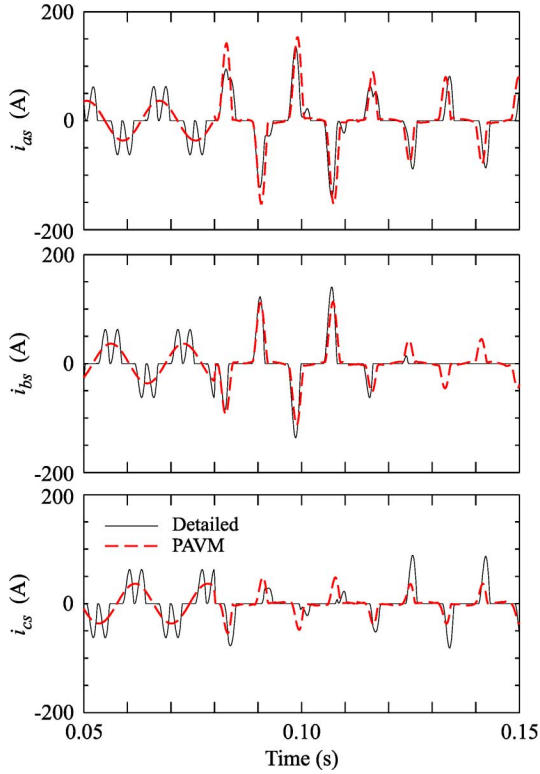


Fig. 8. Transient response of the rectifier system ac phase currents to a change in ac voltages leading to unbalanced operation among the phases in DCM.

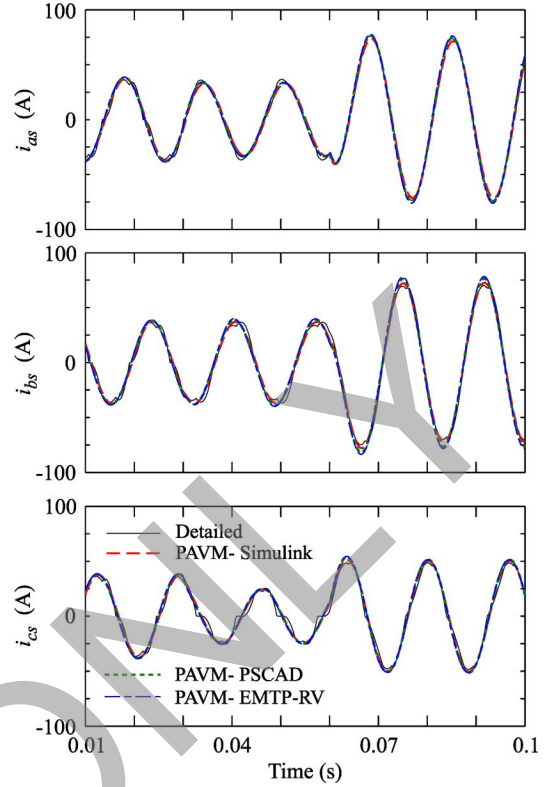


Fig. 10. Transient response of the rectifier system ac phase currents in CCM under unbalanced ac input voltages.

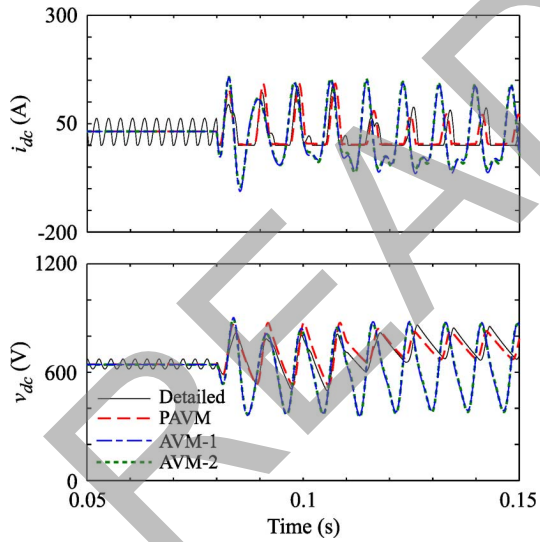


Fig. 9. Transient response of the rectifier system dc current and voltage to a change in ac voltages leading to unbalanced operation in DCM.

fluctuation produced by the detailed simulation of the rectifier system.

B. Unbalanced Operation in CCM

To implement the CCM, the input ac filter is added to the system, and the dc capacitor is removed. In the following study, the rectifier is assumed to start in CCM-1 with a balanced three-phase source and a resistive load $R_L = 15 \Omega$. At $t = 0.03$ s, the

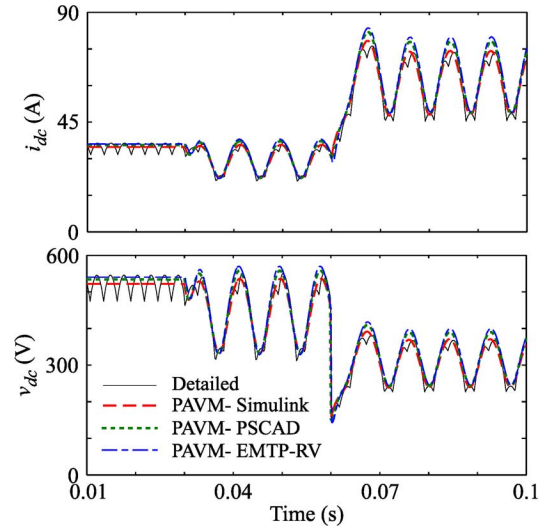


Fig. 11. Transient response of the dc current and voltage of the rectifier system in CCM under unbalanced ac input voltages.

magnitude of e_{cs} is reduced by half leading to unbalanced operation among the rectifier phases. Then, at $t = 0.06$ s, the load is stepped to $R_L = 5 \Omega$, which changes the mode to CCM-2. The resulting ac phase currents predicted by all models are illustrated in Fig. 10. The corresponding dc bus current and voltage are shown in Fig. 11. Due to limited space, only the results of PAVM and the detailed model are illustrated. The results of PAVM obtained using PSCAD, EMTP-RV, and Simulink are all superimposed, and are essentially identical. The PAVM predicts the unbalanced operation of dc and ac variables quite well.

TABLE III
COMPARISON OF SIMULATION TIME STEPS OF DIFFERENT MODELS

Model	Step Size, Δt	# Time Steps
Detailed - PSCAD	50 μs	2,001
Detailed - Simulink	1 ms (max)	1,042
PAVM - PSCAD	200 μs	501
PAVM - EMTP-RV	300 μs	334
PAVM - Simulink	1 ms (max)	247

We also compare the time steps needed for simulation by various models. The number of time steps taken by the considered models for the study of Figs. 10 and 11 is summarized in Table III. In PSCAD, the detailed model is run by using the typical EMTP time step of 50 μs . In Simulink, a variable-step solver ODE15s has been used which dynamically adjusts the time-step size and may therefore require fewer time steps as seen in Table III. Here, the maximum allowable time step of 1 ms and absolute and relative tolerances of 1e-4 have been used. As seen in Table III, the PAVMs implemented in PSCAD, EMTP-RV, and Simulink require much fewer time steps and are therefore significantly faster than the respective detailed models. For consistency, the PAVM-Simulink model was run with the same solver, ODE15s, step size limits, and tolerances as the corresponding detailed model. To obtain a similar result, the PAVM in PSCAD and EMTP-RV had to use a time step of 200 and 300 μs , respectively.

VIII. CONCLUDING REMARKS

This paper gives an overview of dynamic average modeling of the front-end rectifier load systems. The typical configurations of the three-phase front-end rectifier with and without the smoothing ac choke inductor, and variations of the dc filter, are also discussed and shown to result in the two most common operating modes (i.e., DCM and CCM). The models AVM-1 and AVM-2 can be used quite effectively for the transient studies in CCM-1 under balanced as well as unbalanced conditions among the ac phases. The PAVM model is shown to have good accuracy over a wider range covering DCM and all submodes of CCM, under balanced and unbalanced input ac voltages. The presented models have been implemented in PSCAD/EMTDC, EMTP-RV, and Matlab/Simulink, which are commonly used for conducting transient studies. The presented models, studies, and the literature review will be useful to the researchers and practicing engineers who are actively using digital programs and transient simulation tools for modeling and analyzing power systems containing front-end rectifiers.

APPENDIX

Medium power front-end rectifier system parameters:
 $\sqrt{3}E = 480$ V, $f_e = 60$ Hz, $r_{th} = 0.01$ Ω , $L_{th} = 500$ μH ,
 $r_{ac} = 0.091$ Ω , $L_{ac} = 9.545$ mH, $r_{dc} = 0$, $L_{dc} = 0$,
 $C = 500$ μF .

REFERENCES

- [1] B. Wu, *High-Power Converters and AC Drives*. Piscataway, NJ: IEEE Press, 2006.
- [2] K. Lee, V. Blasko, T. M. Jahns, and T. A. Lipo, "Input harmonic estimation and control methods in active filters," *IEEE Trans. Power Del.*, vol. 25, no. 2, pp. 953–960, Apr. 2010.
- [3] M. E. Villablanca and J. I. Nadal, "Current distortion reduction in six-phase parallel-connected AC/DC rectifiers," *IEEE Trans. Power Del.*, vol. 23, no. 2, pp. 953–959, Apr. 2008.
- [4] K. Lee, G. Venkataramanan, and T. M. Jahns, "Source current harmonic analysis of adjustable speed drives under input voltage unbalance and sag conditions," *IEEE Trans. Power Del.*, vol. 21, no. 2, pp. 567–576, Apr. 2006.
- [5] B. Singh, G. Bhuvaneswari, and V. Garg, "Power-quality improvements in vector-controlled induction motor drive employing pulse multiplication in ac-dc converters," *IEEE Trans. Power Del.*, vol. 21, no. 3, pp. 1578–1586, Jul. 2006.
- [6] G. W. Chang and S. K. Chen, "An analytical approach for characterizing harmonic and interharmonic currents generated by VSI-fed adjustable speed drives," *IEEE Trans. Power Del.*, vol. 20, no. 4, pp. 2585–2593, Oct. 2005.
- [7] M. B. Rifai, T. H. Ortmeier, and W. J. McQuillan, "Evaluation of current interharmonics from AC drives," *IEEE Trans. Power Del.*, vol. 15, no. 3, pp. 1094–1098, Jul. 2000.
- [8] J. Jiang and J. Holtz, "An efficient braking method for controlled ac drives with a diode rectifier front end," *IEEE Trans. Ind. Appl.*, vol. 37, no. 5, pp. 1299–1305, Sep. 2001.
- [9] F. Wang *et al.*, "Analysis and design optimization of diode front-end rectifier passive components for voltage source inverters," *IEEE Trans. Power Electron.*, vol. 23, no. 5, pp. 2278–2289, Sep. 2008.
- [10] J. G. Hwang, P. W. Lehn, and M. Winkelkemper, "A generalized class of stationary frame-current controllers for grid-connected ac-dc converters," *IEEE Trans. Power Del.*, vol. 25, no. 4, pp. 2742–2751, Oct. 2010.
- [11] M. E. Haque, M. Negnevitsky, and K. M. Muttagi, "A novel control strategy for a variable-speed wind turbine with a permanent-magnet synchronous generator," *IEEE Trans. Ind. Appl.*, vol. 46, no. 1, pp. 331–339, Jan./Feb. 2010.
- [12] R. S. Bhide, S. V. Kulkarni, and P. B. Bhandarkar, "Analysis of five-legged transformer used for parallel operation of rectifiers by coupled circuit field approach," *IEEE Trans. Power Del.*, vol. 26, no. 2, pp. 607–616, Apr. 2011.
- [13] P. Ladoux, G. Postiglione, H. Foch, and J. Nuns, "A comparative study of AC/DC converters for high-power DC arc furnace," *IEEE Trans. Ind. Electron.*, vol. 52, no. 3, pp. 747–757, Jun. 2005.
- [14] Y. Suh, H. Park, Y. Lee, and P. K. Steimer, "A power conversion system for AC furnace with enhanced arc stability," *IEEE Trans. Ind. Appl.*, vol. 46, no. 6, pp. 2526–2535, Nov./Dec. 2010.
- [15] G. W. Chang, H. Wang, G. Chuang, and S. Chu, "Passive harmonic filter planning in a power system with considering probabilistic constraints," *IEEE Trans. Power Del.*, vol. 24, no. 1, pp. 208–218, Jan. 2009.
- [16] H. M. Zubi, R. W. Dunn, and F. V. P. Robinson, "Comparison of different common passive filter topologies for harmonic mitigation," in *Proc. Univ. Power Eng. Conf.*, Aug./Sep. 2010, pp. 1–6.
- [17] P. C. Krause and T. A. Asipo, "Analysis and simplified representations of rectifier-inverter reluctance synchronous motor drives," *IEEE Trans. Power App. Syst.*, vol. PAS-88, no. 6, pp. 962–970, Jun. 1969.
- [18] E. D. Eyman and Y. V. Kolchev, "Universal analog computer model for three-phase controlled rectifier bridges," *IEEE Trans. Power App. Syst.*, vol. PAS-95, no. 4, pp. 1136–1144, Jul. 1976.
- [19] Alternative Transients Programs ATP-EMTP, ATP User Group, 2007. [Online]. Available: <http://www.emtp.org>
- [20] Electromagnetic Transient Program EMTP RV, CEA Technologies, Inc., 2007. [Online]. Available: <http://www.emtp.com>
- [21] PSCAD/EMTDC Ver. 4.0 On-Line Help Manitoba HVDC Research Centre and RTDS Technologies Inc. Winnipeg, MB, Canada, 2005.
- [22] "Simulink Dynamic System Simulation Software, Users Manual" MathWorks Inc., Natick, MA, 2008. [Online]. Available: <http://www.mathworks.com>
- [23] S. Chiniforoosh, J. Jatskevich, A. Yazdani, V. Sood, V. Dinavahi, J. A. Martinez, and A. Ramirez, "Definitions and applications of dynamic average models for analysis of power systems," *IEEE Trans. Power Del.*, vol. 25, no. 4, pp. 2655–2669, Oct. 2010.
- [24] J. Pedra, F. Corcoles, and F. J. Suelves, "Effects of balanced and unbalanced voltage sags on VSI-fed adjustable-speed drives," *IEEE Trans. Power Del.*, vol. 20, no. 1, pp. 224–233, Jan. 2005.
- [25] S. D. Pekarek, O. Wasynczuk, and H. J. Hegner, "An efficient and accurate model for the simulation and analysis of synchronous machine/converter systems," *IEEE Trans. Energy Convers.*, vol. 13, no. 1, pp. 42–48, Mar. 1998.

- [26] S. D. Pekarek and E. A. Walters, "An accurate method of neglecting dynamic saliency of synchronous machines in power electronic based systems," *IEEE Trans. Energy Convers.*, vol. 14, no. 4, pp. 1177–1183, Dec. 1999.
- [27] L. Wang and J. Jatskevich, "A voltage-behind-reactance synchronous machine model for the EMTP-type solution," *IEEE Trans. Power Syst.*, vol. 21, no. 4, pp. 1539–1549, Nov. 2006.
- [28] N. Mohan, T. M. Undeland, and W. P. Robbins, *Power Electronics: Converters, Applications and Design*, 2nd ed. New York: Wiley, 1995.
- [29] A. M. De Broe, S. Drouilhet, and V. Gevorgian, "A peak power tracker for small wind turbines in battery charging applications," *IEEE Trans. Energy Convers.*, vol. 14, no. 4, pp. 1630–1635, Dec. 1999.
- [30] K. L. Lian, B. K. Perkins, and P. W. Lehn, "Harmonic analysis of a three-phase diode bridge rectifier based on sampled-data model," *IEEE Trans. Power Del.*, vol. 23, no. 2, pp. 1088–1096, Apr. 2008.
- [31] M. Grotzbach and R. Reiner, "Line current harmonics of VSI-fed adjustable-speed drives," *IEEE Trans. Ind. Appl.*, vol. 36, no. 2, pp. 683–690, Mar. 2000.
- [32] G. Carpinelli, F. Iacovone, A. Russo, P. Varilone, and P. Verde, "Analytical modeling for harmonic analysis of line current of VSI-fed drives," *IEEE Trans. Power Del.*, vol. 19, no. 3, pp. 1212–1224, Jul. 2004.
- [33] A. R. Prasad, P. D. Ziogas, and S. Manias, "Passive input current wave-shaping method for three-phase diode rectifiers," *Proc. Inst. Elect. Eng. B, Elect. Power Appl.*, vol. 139, no. 6, pp. 512–520, Nov. 1992.
- [34] I. Barbi, J. C. Fangundes, and C. M. T. Cruz, "A low cost high power factor three-phase diode rectifier with capacitive load," in *Proc. Appl. Power Electron. Conf. Expo.*, Feb. 1994, vol. 2, pp. 745–751.
- [35] B. Pilvelait, T. Ortmeier, and M. Grizer, "Harmonic evaluation of inductor location in a variable speed drive," in *Proc. ICHPS V Int. Conf. Harmon. Power Syst.*, Sep. 1992, pp. 267–271.
- [36] R. M. Davis, *Power Diode and Thyristor Circuits*. Cambridge, MA: Cambridge Univ. Press, 1971.
- [37] P. C. Krause, O. Wasynczuk, and S. D. Sudhoff, *Analysis of Electric Machinery and Drive Systems*, 2nd ed. Piscataway, NJ: IEEE Press, 2002.
- [38] D. Aliprantis, S. D. Sudhoff, and B. T. Kuhn, "A brushless exciter model incorporating multiple rectifier modes and Preisach's hysteresis theory," *IEEE Trans. Energy Convers.*, vol. 21, no. 1, pp. 136–147, Mar. 2006.
- [39] H. Zhu, "New multi-pulse diode rectifier average models for AC and DC power systems studies," Ph.D. dissertation, Virginia Polytech. Inst. State Univ., Blacksburg, VA, 2005.
- [40] H. Zhu *et al.*, "Average modeling of three-phase and nine-phase diode rectifiers with improved ac current and dc voltage dynamics," in *Proc. 31st Annu. Conf. IEEE Ind. Electron. Soc.*, Nov. 2005, pp. 1–6.
- [41] S. D. Sudhoff and O. Wasynczuk, "Analysis and average-value modeling of line-commutated converter-synchronous machine systems," *IEEE Trans. Energy Convers.*, vol. 8, no. 1, pp. 92–99, Mar. 1993.
- [42] S. D. Sudhoff, K. A. Corzine, H. J. Hegner, and D. E. Delisle, "Transient and dynamic average-value modeling of synchronous machine fed load-commutated converters," *IEEE Trans. Energy Convers.*, vol. 11, no. 3, pp. 508–514, Sep. 1996.
- [43] J. T. Alt, S. D. Sudhoff, and B. E. Ladd, "Analysis and average-value modeling of an inductorless synchronous machine load commutated converter system," *IEEE Trans. Energy Convers.*, vol. 14, no. 1, pp. 37–43, Mar. 1999.
- [44] I. Jadric, D. Borojevic, and M. Jadric, "Modeling and control of a synchronous generator with an active DC load," *IEEE Trans. Power Electron.*, vol. 15, no. 2, pp. 303–311, Mar. 2000.
- [45] J. Jatskevich, S. D. Pekarek, and A. Davoudi, "Parametric average-value model of synchronous machine-rectifier systems," *IEEE Trans. Energy Convers.*, vol. 21, no. 1, pp. 9–18, Mar. 2006.
- [46] V. Caliskan, D. J. Perreault, T. M. Jahns, and J. G. Kassakian, "Analysis of three-phase rectifiers with constant-voltage loads," *IEEE Trans. Circuits. Syst. I, Fundam. Theory Appl.*, vol. 50, no. 9, pp. 1220–1226, Sep. 2003.
- [47] P. Pejović and J. W. Kolar, "Exact analysis of three-phase rectifiers with constant voltage loads," *IEEE Trans. Circuits Syst. II, Exp. Briefs*, vol. 55, no. 8, pp. 743–747, Aug. 2008.
- [48] Q. Su and K. Strunz, "Stochastic polynomial-chaos-based average modeling of power electronic systems," *IEEE Trans. Power Electron.*, vol. 26, no. 4, pp. 1167–1171, Apr. 2011.